A Viscoelastic Hybrid Shell Finite Element

Arthur R. Johnson
Vehicle Technology Directorate, MS 240
Army Research Laboratory,
NASA Langley Research Center
Hampton, VA 23681-0001

Abstract

An elastic large displacement thick-shell hybrid finite element is modified to allow for the calculation of viscoelastic stresses. Internal strain variables are introduced at the element's stress nodes and are employed to construct a viscous material model. First order ordinary differential equations relate the internal strain variables to the corresponding elastic strains at the stress nodes. The viscous stresses are computed from the internal strain variables using viscous moduli which are a fraction of the elastic moduli. The energy dissipated by the action of the viscous stresses is included in the mixed variational functional. Nonlinear quasi-static viscous equilibrium equations are then obtained. Previously developed Taylor expansions of the equilibrium equations are modified to include the viscous terms. A predictor-corrector time marching solution algorithm is employed to solve the algebraic-differential equations. The viscous shell element is employed to numerically simulate a stair-step loading and unloading of an aircraft tire in contact with a frictionless surface.

Key words

Viscoelasticity, Hybrid Elements, Tire Models

Introduction

Aircraft tires are composite structures manufactured with viscoelastic materials such as carbon black filled rubber and nylon cords. When loaded, tires experience large deflections and moderately large strains [2]. Finite element models of tires typically employ either two-dimensional thick shell or three-dimensional solid elements [3, 15]. Elastic finite element shell models for tires have been used to predict the shape of tire footprints as a function of loading [10, 13, 14, 18, 19, 20]. Elastic models do not include the viscoelastic nature of the tire which can have a significant effect on load-displacement curves. In this paper the quasi-static viscoelastic loading and unloading of an aircraft tire is numerically simulated. An experimental effort is reported elsewhere [11].

In several previous papers viscoelastic constitutive models have been utilized to determine the dynamic deformations of tires. The following references are provided as a starting point for readers interested in obtaining details about

other viscoelastic finite element models for tires. Padovan, et al. [9, 12, 16] performed an extensive study in which a finite element algorithm was developed for rolling tires. Padovan's model included the effects of large deformations and contact. It also employed fractional derivatives to model the viscoelastic effects. The tire models made by Oden et al. [3, 15] also included the effects of large deformations and contact. However, Oden's model employed the history integral formulation for the viscoelastic effects.

In this paper, internal strain variables are employed to convert an elastic hybrid shell element [14] into a viscous mixed shell element. The model is developed as follows. Internal strain variables are introduced at the stress nodes of the mixed element. First order differential equations relate the internal variables to the physical strain variables. The equations represent a Maxwell solid [4, 5, 6, 7, 21]. Viscous stresses are determined from the internal strains by using material parameters referred to as viscous moduli. An expression for the energy dissipated during deformation is computed from the viscous stresses. This is accomplished by employing the finite element interpolations that are used to compute the stresses from the strains in the elastic version of the shell element. The dissipation energy functional is added to the mixed variational statement for the elastic problem. Nonlinear algebraic equilibrium equations are determined and are numerically solved, simultaneously, with the internal variable differential equations. The numerical predictor-corrector solution procedure employs the Newton-Raphson method for the nonlinear algebraic equations and the trapezoidal method for the differential equations. The tangent matrix required in the Newton-Raphson scheme is a modified version of the previously determined [14, 18, 19, 20] tangent matrix for the nonlinear elastic problem.

At the end of the paper, the viscous shell element is employed in a computational simulation of a stair-step loading and unloading of an aircraft tire.

Viscoelastic Mixed Shell Element

An elastic shell element capable of modeling geometrically nonlinear deformations of thick laminated composites was developed by Noor, et al. [10, 13, 14, 18, 19, 20] Figure 1. shows the physical variables employed to describe the energy in the deformed shell. The elastic finite element has nine displacement nodes with five variables at each node, and four stress nodes with eight variables at each node, see Figure 2. The constitutive model [18, 19, 20] in the shell generalized coordinates is abbreviated as

$$\{\sigma\} = [C]\,\{\epsilon\} \tag{1}$$

where $\{\sigma\} = (N_s, N_\theta, N_{s\theta}, M_s, M_\theta, M_{s\theta}, Q_s, Q_\theta)^T$ is a vector of stress variables, $\{\epsilon\} = (N_s, N_\theta, N_{s\theta}, M_s, M_\theta, M_{s\theta}, Q_s, Q_\theta)^T$ is a vector of the Sanders-Budiansky nonlinear strains[1, 17], and $[C]$ is a matrix of elastic stiffness constants. The elastic element employs the Hellinger-Resiner mixed variational principle which

is constructed as follows. The complementary form of the energy is integrated over the volume of the shell and the total work done by external forces is subtracted. This results in Π_{HR} which is expressed as follows.

$$\Pi_{HR} = \int_{\Omega} \left(\{\sigma\}^T \{\varepsilon\} - \frac{1}{2} \{\sigma\}^T [F] \{\sigma\} \right) d\Omega - W \tag{2}$$

where Ω is the volume of the shell, $[F]$ is a flexibility matrix, and W is the work done by external forces.

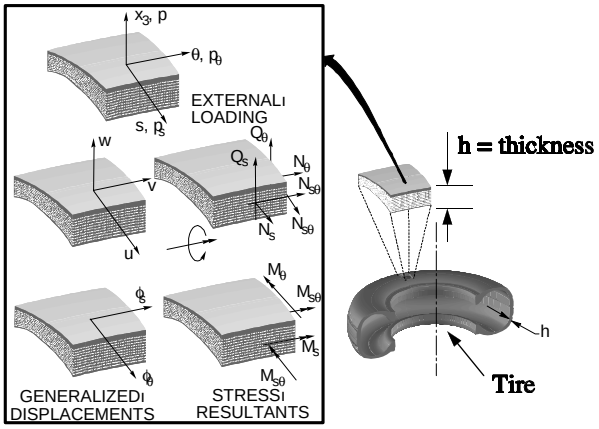

Figure 1. Shell displacement and force variables.

Next, the energy functional, Π_{HR}, is discretized by the finite element method [14]. At the element level, the displacements and stress resultants are approximated by employing interpolation functions with the nodal values shown in Figure 2. The Sanders-Budiansky nonlinear strains are computed and substituted into Equation (2) above. After the volume integration is performed for an element, the Hellinger-Resiner variational expression is given in short-hand notation as follows.

$$\Pi_{HR}^{elt} (\{x\}, \{h\}) = V - U^C - W \tag{3}$$

where $V = \int_{\Omega_{elt}} \{\sigma\}^T \{\varepsilon\} \, d\Omega \equiv \left\{\widehat{h}\right\}^T \left(\left[\widehat{S}_{lx}\right] + \frac{1}{2} \left[\widehat{M}_{nlxx}\right] \right) \equiv \left\{\widehat{h}\right\}^T \{\widehat{\varepsilon}\}$, $U^C = \int_{\Omega_{elt}} \frac{1}{2} \{\sigma\}^T [F] \{\sigma\} \, d\Omega \equiv \frac{1}{2} \left\{\widehat{h}\right\}^T \left[\widehat{F}\right] \left\{\widehat{h}\right\}$, $W = \{\widehat{x}\}^T \{\widehat{p}\} = \{\widehat{p}\}^T \{\widehat{x}\}$, $\{\widehat{x}\}$ and $\{\widehat{\varepsilon}\}$ are vectors containing the element's nodal displacements and strains, $\{h\}$ is an element level vector, $\left[\widehat{S}_{lx}\right]$ and $\left[\widehat{M}_{nlxx}\right]$ are operators that produce the linear and nonlinear contributions to $\{\widehat{\varepsilon}\}$ from the nodal displacements, $\left[\widehat{F}\right]$

is an element level flexibility matrix, and $\{\widehat{p}\}$ represents the consistent applied load vector.

Internal strain variables are employed herein to modify the above formulation making it applicable to a Maxwell type viscoelastic material [6, 7]. Introduce, in vector form, internal strain fields, $\{\varepsilon_{jv}\}$, and matrices of viscous stiffness constants, $[C_{jv}]$, within the element. The viscous stress vector at a point in the element is computed as follows.

$$\{\sigma_v\} = \sum_{j=1}^{n} [C_{jv}] \{\varepsilon_{jv}\} \tag{4}$$

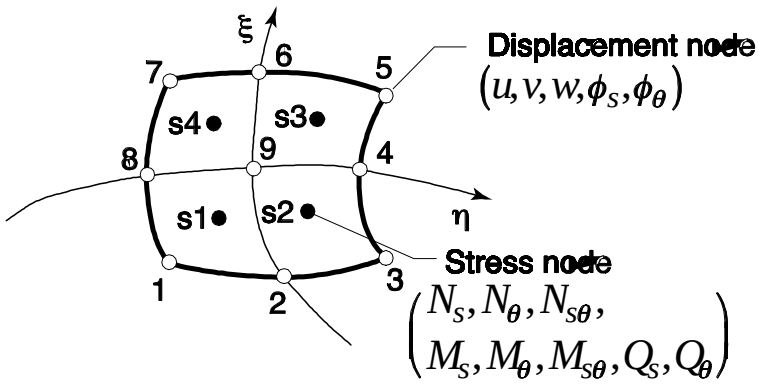

Figure 2. Shell element displacement and stress variables.

The total value of the stress vector, elastic plus viscous, at a point is $\{\sigma_t\} = \{\sigma\} + \{\sigma_v\}$. Next, following the computation of the elastic potential, V , in Equation (3), the energy dissipated by the viscous stresses, Q , throughout the element is computed as follows.

$$Q = \int_{\Omega_{elt}} \{\sigma_v\}^T \{\varepsilon\}\, d\Omega \equiv \left\{\widehat{h_v}\right\}^T \{\widehat{\varepsilon}\} = \left\{\widehat{h_v}\right\}^T \left(\left[\widehat{S}_{lx}\right] + \frac{1}{2} \left[\widehat{M}_{nlxx}\right] \right) \tag{5}$$

where $\left\{\widehat{h_v}\right\}$ is an element level vector. The mixed variational functional for the viscous element, $\Pi_{HR}^{elt,v}$, is given by

$$\Pi_{HR}^{elt,v} = V + Q - U^C - W \tag{6}$$

The model is completed by relating the rate of change of the internal strain variables to the physical strain variables. Here we employ a simple form of the Maxwell solid theory by requiring the following differential equations to be satisfied [6, 7, 4].

$$\frac{d\left\{\widehat{\varepsilon}_{jv}\right\}}{dt}+\frac{\left\{\widehat{\varepsilon}_{jv}\right\}}{\tau_j}=\frac{d\left\{\widehat{\varepsilon}\right\}}{dt} \tag{7}$$

Equations (4) and (7) determine the viscous stresses for a time dependent deformation of the element, $\{\widehat{x}\,(t)\}$. Note, an advantage of this algorithm is that a variety of viscoelastic models can be employed by simply changing Equation (7).

At each instant of time, the element equilibrium equations are given by the first variation of , Equation (6). The equilibrium equations are

$$\left\{f_{\widehat{h}}\left(\{\widehat{x}\},\left\{\widehat{h}\right\}\right)\right\}=\left(\left[\widehat{S}_{lx}\right]+\frac{1}{2}\left[\widehat{M}_{nlxx}\right]\right)-\left[\widehat{F}\right]\left\{\widehat{h}\right\}=\{0\} \tag{8}$$

and

$$\left\{f_{\widehat{x}}\left(\{\widehat{x}\},\left\{\widehat{h}\right\}\right)\right\}=\left(\left[\widehat{S}_{l}\right]+\frac{1}{2}\left[\widehat{M}_{nlx}\right]\right)^{T}\left(\left\{\widehat{h}\right\}+\left\{\widehat{h}_{v}\right\}\right)-\{\widehat{p}\}=\{0\} \tag{9}$$

where $\left[\widehat{S}_{l}\right]$ and $\left[\widehat{M}_{nlx}\right]$ are the derivatives of the operators $\left[\widehat{S}_{lx}\right]$ and $\left[\widehat{M}_{nlxx}\right]$ with respect to the element displacement variables, $\{\widehat{x}\}$. Equations (8) and (9) are assembled by standard methods to obtain the global equilibrium equations. The global equations are then solved simultaneously with Equation (7) (for all elements.)

The Taylor expansion of Equations (8) and (9) produces the element's tangent matrix. The resulting element level Newton-Raphson equations for the increments of the variables $\Delta\{\widehat{x}\}$ and $\Delta\left\{\widehat{h}\right\}$ are given below.

$$\begin{bmatrix} -\left[\widehat{F}\right] & \left(\left[\widehat{S}_{l}\right]+\frac{1}{2}\left[\widehat{M}_{nlx}\right]\right) \\ \left(\left[\widehat{S}_{l}\right]+\frac{1}{2}\left[\widehat{M}_{nlx}\right]\right)^{T} & \left[\widehat{M}_{nl}\right]\left(\left\{\widehat{h}\right\}+\left\{\widehat{h}_{v}\right\}\right) \end{bmatrix}\begin{Bmatrix} \Delta\left\{\widehat{h}\right\} \\ \Delta\{\widehat{x}\} \end{Bmatrix}=\begin{Bmatrix} \left\{f_{\widehat{h}}\right\} \\ \left\{f_{\widehat{x}}\right\} \end{Bmatrix} \tag{10}$$

where $\left[\widehat{M}_{nl}\right]$ is the second derivative of the operator $\left[\widehat{M}_{nlxx}\right]$ with respect to the nodal displacements. Equations (10) are assembled for all elements and solved to provide estimates of the variables increments across a time step. The new elastic strains at the end of the time step are computed at all stress nodes. The internal strain variables are then estimated at the end of the time step by employing the trapezoidal method to Equation (7). Next, global equilibrium is checked. If equilibrium is not satisfied the process is repeated. When equilibrium is satisfied the required output is computed and the time is advanced.

Tire Stair-Step Loading Simulation

The aircraft tire modeled below is a 32 x 8.8, type VII, bias-ply Shuttle nose-gear tire which has a 20-ply rated carcass and a maximum speed rating of 217 knots [11, 18, 19, 20]. The tread pattern consists of three circumferential grooves and the rated inflation pressure is 320 psi.

The details of the tire's elastic material model are described by Tanner [18]. The tire is a cord-rubber composite and was treated as a laminated material. It was divided into seven regions in the direction of the meridian (from the center of the tread region to the rim.) Tire thickness, properties of the plies, etc. were measured and tabulated. Elastic constants were computed by the law of mixtures to obtain linear orthotropic stress-strain constitutive models for each layer. These properties were transformed to the shell coordinate system and integrated through the thickness of the shell elements.

The viscous material model employed was determined by least-square fitting tire load-relaxation data [8] to a Prony series of the form

$$f_v(t) = \left(\sum_{j=1}^{3} \alpha_j \, e^{\frac{-t}{\tau_j}} \right) f_v(0) \tag{11}$$

where $f_v(t)$ is the relaxing component of the load, $f_v(0)$ is the initial load, τ_{jv} are the constants in Equations (7), and α_j are factors of the products $[C_{jv}]\{\varepsilon_{jv}\}$ so that Equation (4) becomes

$$\{\sigma_v\} = \sum_{j=1}^{n} \alpha_j [C] \{\varepsilon_{jv}\} \tag{12}$$

The values of the constants found by Johnson et al. [8] and used here are $\{(\alpha_j, \tau_j)\}_{j=1}^{3} = \{(0.01836,\ 10), (0.01630,\ 100), (0.03650,\ 1000)\}$.

The tire's finite element mesh and a sketch of the frictionless loading platform are shown in Figure 3. The mesh is similar to the "Model 1" mesh employed by Tanner [18]. The elastic model has 540 elements and 28,565 degrees of freedom (not including the Lagrange multipliers used for points that come into contact.) An additional 103,680 internal variables were added to program the solution algorithm for the material model described above. Computed elastic and viscoelastic load-displacement curves, obtained by enforcing a stair-step tire rim displacement are shown in Figure 4. The finite element load-displacement hysteresis loop is shown in Figure 5.

Concluding Remarks

An algorithm for converting elastic structural elements based on the Hellinger-Resiner mixed variational principle to viscoelastic structural elements was presented. The thirteen node large displacement thick-shell element derived by Noor and Hartley [14] was employed to describe the algorithm. A finite element

tire model based on this shell element, and used by Tanner [18, 19, 20] to analyze tire footprints, was modified so that the tire material would represent a Maxwell solid. A stair-step tire loading and unloading was numerically simulated. The new computational algorithm functioned successfully.

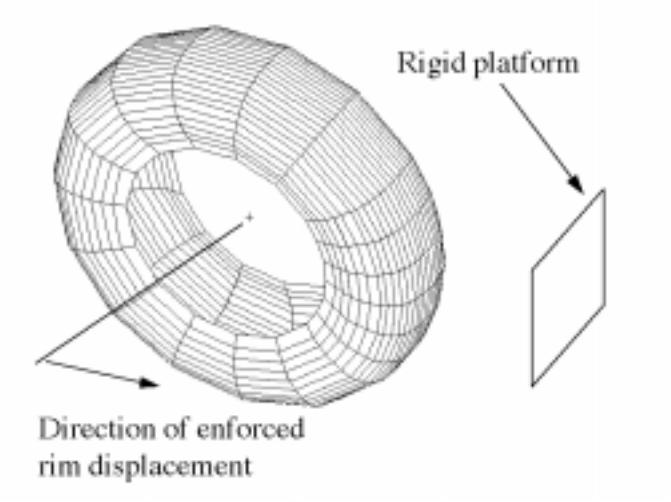

Figure 3. Tire finite element model.

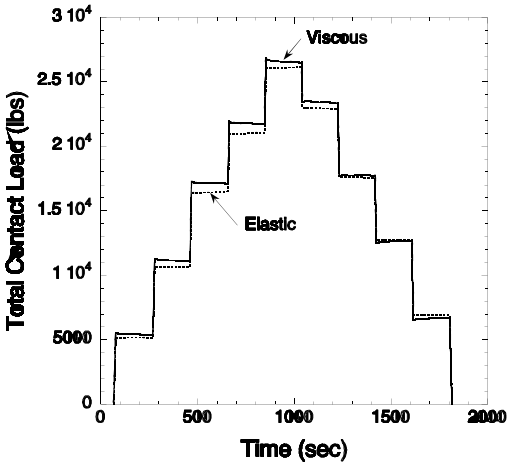

Figure 4. Computed viscous and elastic tire loads.

Acknowledgment

The author would like to thank Ms. Jeanne M. Peters of the Center for Advanced Computational Technology, University of Virginia, NASA Langley Research Center for assisting with the modifications of the finite element code. Also, the author is grateful to the United States Army Research Standardization Group, Europe for supporting his participation in MAFELAP99 and to the Army Research Laboratory at the NASA Langley Research Center for supporting this research.

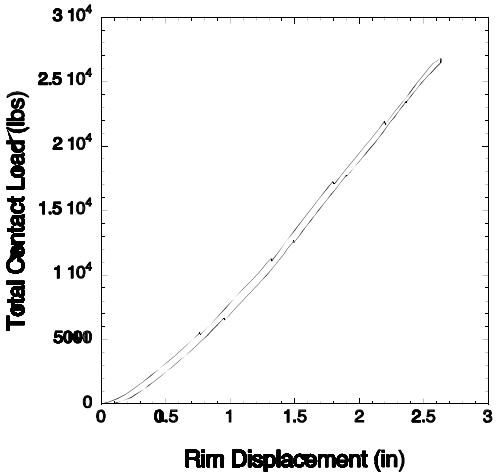

Figure 5. Finite element hysteresis curve.

References

[1] B. Budiansky (1968). Notes on Nonlinear Shell Theory. *J. Appl. Mech.*, Vol. 35, No. 2: 393–401.

[2] S. K. Clark (1981), Mechanics of Pneumatic Tires. *US Government Printing Office*, 475–540.

[3] L. O. Faria, J. M. Bass, and J. T. Oden (1989). A Three-Dimensional Rolling Contact Model for a Reinforced Rubber Tire. *Tire Science and Technology, TSTCA*, Vol. 17, No. 3: 217–233.

[4] A. R. Johnson (1999). Modeling Viscoelastic Materials Using Internal Variables. *The Shock and Vibration Digest*, Vol. 31, No. 2: 91–100.

[5] A. R. Johnson and R. G. Stacer (1993). Rubber viscoelasticity using the physically constrained system's stretches as internal variables. *ACS, Rubber Chemistry and Technology*, Vol. 66, No. 4: 567–577.

[6] A. R. Johnson and A. Tessler (1997). A Viscoelastic Higher-Order Beam Finite Element. *The Mathematics of Finite Elements and Applications, Highlights 1996, Ed. J. R. Whiteman, Wiley, Chichester*, 333–345.

[7] A. R. Johnson, A. Tessler, and M. L. Dambach (1997). Dynamics of Thick Viscoelastic Beams. *ASME J. Engng and Matls Tech*, Vol. 119: 273–278.

[8] A. R. Johnson, J. A. Tanner, and A. J. Mason (1999). Quasi-Static Viscoelastic Finite Element Model of an Aircraft Tire. *NASA/TM-1999-209141.*

[9] R. Kennedy and J. Padovan (1987). Finite Element Analysis of Steady and Transiently Moving/Rolling Nonlinear Viscoelastic Structure - II, Shell and Three Dimensional Simulations. *Computers and Structures*, Vol. 27, No. 2: 259–273.

[10] K. O. Kim, J. A. Tanner, A. K. Noor, and M. P. Robertson (1991). Computational Methods for Frictionless Contact with Application to Space Shuttle Orbitor Nose-Gear Tires, . *NASA/TP-1991-3073.*

[11] A. J. Mason, J. A. Tanner, and A. R. Johnson (1997). Quasi-Static Viscoelasticity Loading Measurements of an Aircraft Tire. *NASA/TM-1997-4779, ARL/TR-1402.*

[12] Y. Nakajima and J. Padovan (1987). Finite Element Analysis of Steady and Transiently Moving/Rolling Nonlinear Viscoelastic Structure - III, Impact/Contact Simulations. *Computers and Structures*, Vol. 27, No. 2: 275–286.

[13] A. K. Noor, C. M. Anderson, and J. A. Tanner (1987). Exploiting Symmetries in the Modeling and Analysis of Tires. *NASA/TP-1987-2649.*

[14] A. K. Noor and S. J. Hartley (1977). Nonlinear Shell Analysis via Mixed Isoparametric Elements. *Computers and Structures*, Vol. 7: 615–626.

[15] J. T. Oden, T. L. Lin, and J. M. Bass (1988). A Finite Element Analysis of the General Rolling Contact Problem for a Viscoelastic Rubber Cylinder. *Tire Science and Technology, TSTCA*, Vol. 16, No. 1: 18–43.

[16] J. Padovan (1987). Finite Element Analysis of Steady and Transiently Moving/Rolling Nonlinear Viscoelastic Structure - I Theory. *Computers and Structures*, Vol. 27, No. 2: 249–257.

[17] J. L. Sanders (1963). Nonlinear Theories for Thin Shells. *Q. Appl. Math.*, Vol. 21., No. 1: 21–36.

[18] J. A. Tanner (1996). Computational Methods for Frictional Contact with Application to the Space Shuttle Orbiter Nose-Gear Tire, Comparisons of Experimental Measurements and Analytical Predictions. *NASA/TP-1996-3573.*

[19] J. A. Tanner (1996). Computational Methods for Frictional Contact with Application to the Space Shuttle Orbiter Nose-Gear Tire, Development of Frictional Contact Algorithm. *NASA/TP-1996-3574*.

[20] J. A. Tanner, V. J. Martinson, and M. P. Robinson (1994). Static Frictional Contact of the Space Shuttle Nose-Gear Tire. *Tire Science and Technology, TSTCA*, Vol. 22, No. 4: 242–272.

[21] I. M. Ward (1983). *Mechanical Properties of Solid Polymers, Wiley and Sons.*